Similarity relations for anisotropic scattering in absorbing media

Graaff, Reindert; Aarnoudse, Jan G; de Mul, Frits F M; Jentink, Henk W

Published in:
Optical engineering

DOI:
10.1117/12.60735

Publication date:
1993

Similarity relations for anisotropic scattering in absorbing media

Reindert Graaff
Jan G. Aarnoudse
University of Groningen
Centre for Biomedical Technology
Department of Obstetrics and Gynecology
Oostersingel 59
9713 EZ Groningen, The Netherlands

Frits F. M. de Mul
Henk W. Jentink*
University of Twente
Faculty of Applied Physics
P.O. Box 217
7500 AE Enschede, The Netherlands

Abstract. The validity of the similarity parameter $\Sigma_s' \equiv \Sigma_s(1-g)$, the reduced scattering coefficient, where g is the average cosine of the scattering phase function is investigated. Attenuation coefficients α and diffusion patterns are obtained from solutions of the transport equation for isotropic scattering and Rayleigh-Gans scattering, applied to infinite media. Similarity is studied for the attenuation coefficient α, as well as for the Kubelka-Munk absorption and backscattering coefficients in the positive and negative directions, and for predictions of the internal reflection at interfaces. Similarity between solutions of the Boltzmann equation for highly forward scattering and isotropic scattering ($g=0$) exist only when $\Sigma_a \ll \Sigma_s(1-g)$. However, because similarity between results, both with $g>0.9$, is independent of the value of the absorption coefficient, it is advantageous to simulate highly forward scattering media like biological tissues with $g>0.9$, e.g., by Monte Carlo simulations, instead of using isotropic scattering or diffusion theory. Monte Carlo simulations on slabs confirm the deviations from the diffusion approximation and show the behavior near boundaries. Application of similarity may save calculation time in Monte Carlo simulations, because simulation with a lower value for g will increase the mean free path.

Subject terms: biomedical optics; Monte Carlo simulations; transport theory; diffusion approximations; diffusion patterns; attenuation coefficients; anistropic scattering.

Optical Engineering 32(2), 244–252 (February 1993).

1 Introduction

Light propagation in scattering and absorbing media is important in medicine for tissue ablation or photon radiation therapy as well as for noninvasive measurement of properties such as blood flow using laser Doppler flowmetry,[1] cell metabolism using near-infrared spectroscopy,[2] and oxygen saturation of arterial blood using pulse oximetry by transmission[3] or reflection.[4,5]

Several models for light propagation have been applied in tissue optics. In many cases, the diffusion approximation of transport theory has been used,[6–9] which is valid only for isotropic scattering as long as the scattering coefficient Σ_s is much larger than the absorption coefficient Σ_a and as long as the distance between light source and detector is larger than the mean free path (mfp),[8] with $\text{mfp} = 1/(\Sigma_a + \Sigma_s)$. It is possible to avoid the limitations of the diffusion approximation, e.g., by application of Monte Carlo simulations.[1,8] However, Monte Carlo simulations need very long calculation times, especially if $\Sigma_a \ll \Sigma_s$. Other methods have also been reported, such as corrections of the diffusion theory, based on Monte Carlo simulations,[10] and the adding-doubling method, described by Van de Hulst[11] and worked out for Henyey-Greenstein scattering in slabs.[12]

Our primary aim is the development of reflection pulse oximetry, which can be used to monitor the arterial oxygen saturation of the fetus during labor.[5] In pulse oximetry, changes in light intensity, caused by arterial pressure pulses, are measured at two wavelengths, e.g., at 660 and 940 nm. These relative changes in light intensity are roughly proportional to the absorption coefficient of the pulsatile blood volume and the change in blood volume. Because the ratio of absorption coefficients of blood at these wavelengths is a unique function of oxygen saturation, it is possible to determine the arterial oxygen saturation,[3] provided that the influence of light scattering onto the predicted oxygen saturation is restricted.

Pulse oximetry might, in principle, be influenced by arterial and venous blood volume fractions, the absorption and scattering coefficients of tissue as well as arterial and venous blood at the applied wavelengths, and the angular phase functions of blood and tissue for both wavelengths.

*Present address: National Aerospace Laboratory NLR, Aircraft Instrumentation Department, P.O. Box 90502, 1006 BM Amsterdam, The Netherlands.

Paper BM-043 received July 1, 1992; revised manuscript received Sep. 25, 1992; accepted for publication Oct. 8, 1992. This paper is a revision of a paper presented at the SPIE conference on Scattering and Diffraction, September 1988, Hamburg, Germany. The paper presented there appears (unrefereed) in SPIE Proceedings Vol. 1029.

It is not practical to study the influence of light scattering on pulse oximetry by varying all these properties. It is, therefore, necessary to reduce the number of variables involved, which is one of the main aims of the present study.

Similarity[11] has been widely applied to model anisotropic scatterers using isotropic scattering with a reduced scattering coefficient, $\Sigma_s' \equiv \Sigma_s(1-g)$. Here, g is the average cosine of the scattering angle. This model is based on the fact that forwardly peaked scattering (described with a delta function) can be added to isotropic scattering without changing the scattering properties of the medium. However, the validity of the supposed similarity between different anisotropic phase functions and this so-called transport approximation is rather uncertain. Remarkable differences near the boundary between calculation results for anisotropic scattering and the isotropic scattering transport approximation have been reported,[13] even if $\Sigma_a/\Sigma_s' < 0.1$. Such deviations are in agreement with earlier findings of Groenhuis et al.[8] and Van de Hulst.[11] Similar deviations are expected to occur in whole blood.

Recently, we published the results of a study on spherical Rayleigh-Gans scatterers with different aspect ratios, $0 < x < 50$, with $x \equiv 2\pi a/\lambda$, where a is the sphere radius and λ is the wavelength outside the sphere. Results of the more rigorous solution of the Boltzmann transport equation were compared in that study with results of the diffusion approximation.[14] That study provided quantitative data on correction multipliers for the attenuation coefficient α when using diffusion theory. Correction factors for the Kubelka-Munk absorption and backscattering coefficients K and S, respectively, were also given in that study. All correction factors confirmed the validity of the diffusion approximation when $\Sigma_a/\Sigma_s' \ll 1$.

One main aim of the present study is to investigate the range of validity of the similarity rule for Rayleigh-Gans scattering. The numerical results of our previous study[14] are therefore used in the present study (Sec. 3). Another aim of this study is to investigate the validity of the diffusion approximation and whether the correction factors for the attenuation coefficient and Kubelka-Munk coefficients can be used to obtain improved results when applied to light propagation, e.g., in slabs.

2 Theory

2.1 *Boltzmann Transport Equation*

The basic equation in transport theory is the Boltzmann transport equation, a balance equation for the radiance Ψ in the direction Ω. The homogeneous transport equation,

$$\mu \frac{d\Psi(z,\mu)}{(\Sigma_a+\Sigma_s)\,dz} + \Psi(z,\mu) = \frac{c}{2}\int_{4\pi} f(\Omega\cdot\Omega')\Psi(z,\Omega')\,d\Omega' \quad , \quad (1)$$

can be solved for the plane symmetry in an unbounded medium illuminated[11,15,16] at $z=-\infty$. The cosine of the angle with the z axis is represented by μ and the albedo by $c \equiv \Sigma_s/(\Sigma_a+\Sigma_s)$. The angular phase function of the scatterer, $f(\Omega\cdot\Omega')$, obeys

$$\int_{4\pi} f(\Omega\cdot\Omega')\,d\Omega' = 1 \quad . \quad (2)$$

Because of translational invariance of the diffusion pattern, the solution of the homogeneous transport equation is described with

$$\Psi(z,\mu) = \Phi(\mu)\,\exp[-(\Sigma_a+\Sigma_s)z/\nu] = \Phi(\mu)\,\exp(-\alpha z) \quad . \quad (3)$$

Equation (3) shows that the attenuation of the intensity in the z direction is exponential, where $\alpha = (\Sigma_a+\Sigma_s)/\nu$ is the attenuation coefficient. The angular dependent term $\Phi(\mu)$ gives the diffusion pattern. Substitution of Eq. (3) into Eq. (1) yields

$$1 - c\nu\sum_{i=0}^{N}(2i+1)f_i\phi_i Q_i(\nu) = 0 \quad . \quad (4)$$

The largest value of ν for which Eq. (4) is valid is regarded as the solution because it is the mode that is least damped.[11] The expansion coefficients of the phase function, f_i with $i=1, \ldots, N$, are discussed in more detail in Sec. 2.2. The terms $Q_i(\nu)$ are Legendre polynomals[17] of the second kind and of the order i. The terms ϕ_i are given by a recursion relation:

$$\phi_i = \nu(1-cf_{i-1})\phi_{i-1}\frac{2i-1}{i} - \frac{i-1}{i}\phi_{i-2} \quad , \quad (5)$$

with $\phi_0 = 1$ and $\phi_1 = \nu(1-c)$. The solution for the diffusion pattern, the angular distribution of light at any location within the unbounded medium, is given by

$$\Phi(\mu) = \frac{c\nu}{2(\nu-\mu)}\sum_{i=0}^{N}(2i+1)f_i\phi_i P_i(\mu) \quad , \quad (6)$$

where the terms P_i are Legendre polynomals[17] of the first kind and of the order i. In our calculations, we applied $N=50$.

Analytical solutions of these equations can be found for only a few special cases. Recently, Haltrin[18] found an analytical expression for which the diffusion pattern is described with a Henyey-Greenstein function. However, this determines the shape of the phase function. In most cases, a numerical solution of the equations is required.

2.2 *Phase Functions*

In this study, the phase function is derived from Rayleigh-Gans scattering theory:

$$f(\mu)/f(1) = \frac{1+\mu^2}{2}\left\{\frac{3}{(ua)^3}[\sin(ua) - ua\cos(ua)]\right\}^2 \quad , \quad (7)$$

with $ua = 2x\sin(\theta/2)$. The angle θ is the angle between the direction of the photon before and after scattering and $\mu = \cos(\theta)$ in Eqs. (7) to (9). The aspect ratio is represented by x. The value $f(1)$ for a given aspect ratio is found after substitution of Eq. (7) into Eq. (2).

The expansion coefficients are found by numerical integration:

$$f_i = 2\pi\int_{-1}^{1} f(\mu)P_i(\mu)\,d\mu \quad . \quad (8)$$

In many other studies, the Henyey-Greenstein phase function,

$$f(\mu)=\frac{1-g^2}{4\pi(1+g^2-2g\mu)^{3/2}} , \tag{9}$$

is applied. This phase function has been used often, probably because of the simple form of the expansion coefficients: $f_i=g^i$.

2.3 *Kubelka-Munk Absorption and Backscattering Coefficients for the Positive and Negative Directions*

Results obtained with the method described in Sec. 2.1 can be applied to the differential equations for the photon fluxes I and J in the positive and negative directions in the unbounded medium:[19]

$$dI(z)=-K^+I(z)\,dz-S^+I(z)\,dz+S^-J(z)\,dz , \tag{10}$$

$$-dJ(z)=-K^-J(z)\,dz-S^-J(z)\,dz+S^+I(z)\,dz , \tag{11}$$

where K^+ and K^- are the fraction of the flux that are absorbed per unit length in the positive and negative directions, respectively, and S^+ and S^- are the fractions of flux that changes direction per unit length in the positive and negative directions, respectively.

The values of K^+ and K^- are larger than Σ_a because the average photon path length through a slice of the infinite medium with thickness dz is larger than dz and depends on the diffusion pattern. However in diffusion theory and Kubelka-Munk theory, no difference is made between the chances for absorption or (back)scattering in both directions, because it is assumed that the diffusion patterns in both directions does not depend on μ; K and S are used in that case.

In a previous study,[14] we calculated values for K from the diffusion pattern, because K/Σ_a can be interpreted as the average photon path length per unit length dl/dz:

$$K/\Sigma_a=dl/dz=\frac{\int_{-1}^{1}\left|\frac{1}{\mu}\right|\Phi(\mu)|\mu|\,d\mu}{\int_{-1}^{1}\Phi(\mu)|\mu|\,d\mu} . \tag{12}$$

Note that values for K^+/Σ_a and K^-/Σ_a can also be derived from Eq. (12) by integrating over the ranges $0\leq\mu\leq1$ and $-1\leq\mu\leq0$, respectively.

The general solution for I in the unbounded medium is given by Eq. (2), or

$$I(z)=Ae^{-\alpha z} . \tag{13}$$

The ratio between J and I is independent of z in the unbounded medium, because of translational invariance of the diffusion pattern. Substitution in Eqs. (10) and (11) and addition of these equations gives

$$\alpha(I-J)=-\frac{d(I-J)}{dz}=(K^+I+K^-J)=K(I+J) , \tag{14}$$

an expression that is proportional to the sum of the energy fluence rates, photons per unit volume, in the positive and negative directions. The ratio between the fluxes J and I can thus be calculated from α and K, without knowledge of the direction dependence of the properties K and S:

$$\frac{J}{I}=\frac{\alpha-K}{\alpha+K} . \tag{15}$$

Substitution of Eq. (15) into Eq. (10) yields

$$S^+-S^-(J/I)=\alpha-K^+ . \tag{16}$$

This equation shows that S^+ and S^- remain dependent and cannot be derived separately from the equations given above for the unbounded medium.

Therefore, solutions for backscattering coefficients can be found only with additional assumptions. When assuming $K=K^+=K^-$ and $S=S^+=S^-$, substitution of Eq. (13) into Eqs. (10) and (11) yields

$$\alpha^2=K^2+2KS . \tag{17}$$

Based on that assumption, values for S can be derived from the values of α and K, using Eqs. (3) and (12), respectively. Such results can be applied to compare results with Kubelka-Munk theory and diffusion theory.

A better assumption might be that S^+ and S^- are proportional with the average photon path length per unit length in the positive and negative directions, and thus,

$$S^+/K^+\approx S^-/K^- . \tag{18}$$

The relationship between S^+ and S^- is not determined in the present study. It is possible that this relationship is less important in many cases, because it does not influence α and the ratio J/I.

3 Similarity Relations

3.1 *Attenuation Coefficients*

In many studies, the attenuation coefficient α is predicted in the diffusion approximation:

$$\alpha_{diff}=\{3\Sigma_a[\Sigma_a+\Sigma_s(1-g)]\}^{1/2}=[3\Sigma_a(\Sigma_a+\Sigma_s')]^{1/2} . \tag{19}$$

The similarity rule holds for this attenuation coefficient, because α_{diff} depends on Σ_a and Σ_s' only, independent of the chosen phase function. However, with the solution of the transport equation, as given in Sec. 2.1, a more accurate value can be obtained, as shown in a previous study.[14] Because it was shown in that study that the attenuation coefficient in the diffusion approximation α_{diff} is valid for $\Sigma_a\ll\Sigma_s'$, it follows that the similarity rule has to be valid in that range.

To investigate the validity of similarity with respect to α when absorption coefficients are not very small, the data for ratio α_{diff}/α from Ref. 14 are presented in Fig. 1 as a function of the reduced albedo c', with $c'\equiv\Sigma_s'/(\Sigma_a+\Sigma_s')$, instead of the albedo. The results show not only that $\alpha_{diff}/\alpha\approx1$ if $\Sigma_a/\Sigma_s'\approx0$ but also that the curves almost coincide if $x>5$, that is, $g>0.9$. This implies that the similarity rule for α_{diff}/α is valid for large Rayleigh-Gans scatterers, even for small values of c'.

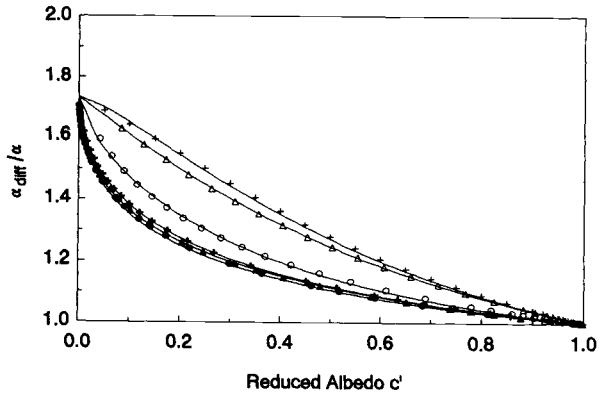

Fig. 1 Ratio between α_{diff}, calculated with the diffusion approximation, and α, calculated with the Boltzmann equation, as a function of the reduced albedo. Isotropic scattering (+) and Rayleigh-Gans scattering for $x=1(\Delta)$, 2(○), 5(+), 10(▲), and 20(●).

3.2 *Diffusion Patterns*

Several diffusion patterns were calculated from Eq. (6), after solving the Boltzmann transport equation, as described above. For an albedo $c=1$, the diffusion pattern for isotropic scattering has a spherical shape. However, for lower values of c, e.g., $c=0.7$ or $c=0.462$, the diffusion pattern resembles elliptically, as shown in Figs. 2(a) and 2(b).

A diffusion pattern for Rayleigh-Gans scattering ($x=20$, $g=0.9913$) was calculated for the same reduced albedo $c'=0.462$ ($c=0.99$). However, the shape deviates, as can be seen from the different curvature at both ends of the pattern in Fig. 2(c). The difference in shape for the same value for c' is caused by the fact that for Rayleigh-Gans scattering, 50 terms in Eq. (5), $N=50$, may contribute to the diffusion pattern, whereas for isotropic scattering only the first term contributes, as $f_i=0$ for $i>0$.

3.3 *Kubelka-Munk Absorption and Backscattering Coefficients*

In a previous study,[14] we derived numerical expressions with tabulated coefficients for K and S as described in Sec. 2.3 for isotropic scattering and Rayleigh-Gans scattering with values of g between 0 and 0.9995 and for the whole range of the albedo between 0 and 1.

To investigate the validity of the similarity rule, some results of K/Σ_a for Rayleigh-Gans scattering are repeated in Fig. 3, however, as a function of c' instead of c. Note that the results deviate from the diffusion approximation result $K_{diff}=2\Sigma_a$ when $c'<1$. The curves for K/Σ_a almost coincide when $x>5$ or $g>0.90$, as in Fig. 1. With Eq. (17), when valid, it would follow that the values for S also coincide in that range.

3.4 *Differentiation between K and S in the Positive and Negative Direction*

From the diffusion patterns in Fig. 2, it can be seen that the average photon path length in the positive direction is different from that in the negative direction, especially for $c'\ll 1$. Therefore, K^+ and K^- were evaluated numerically for isotropic and Rayleigh-Gans scatterers, using Eq. (12) for the positive and negative directions separately. Results

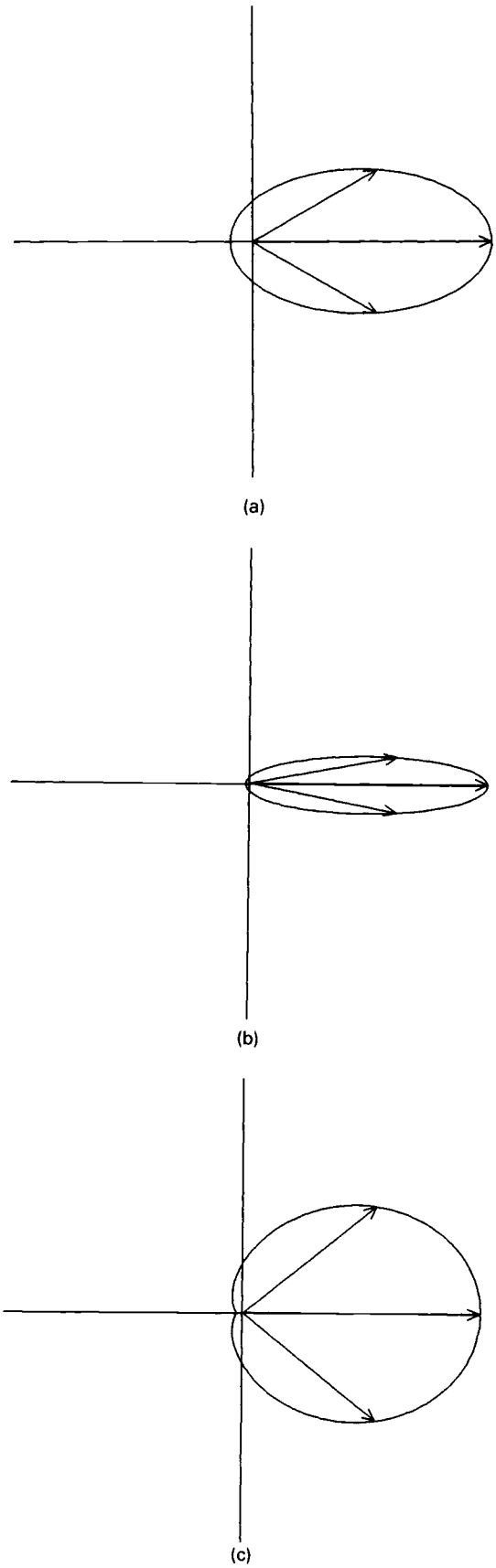

Fig. 2 Diffusion pattern in an infinite medium: (a) isotropic scattering, $c=0.7$; (b) isotropic scattering, $c=0.462$; and (c) Rayleigh-Gans scattering, $x=20$, $c=0.99$, and $c'=0.462$.

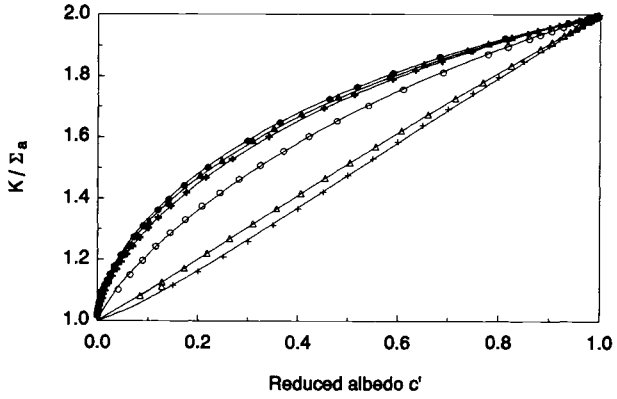

Fig. 3 Results for K/Σ_a as a function of the reduced albedo, calculated from the diffusion pattern: isotropic scattering (+) and Rayleigh-Gans scattering for $x=1(\Delta)$, 2(○), 5(+), 10(▲), and 20(●).

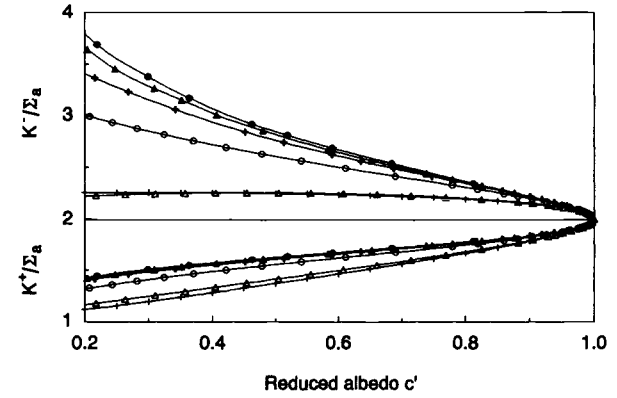

Fig. 4 Results for K^+/Σ_a and K^-/Σ_a as a function of the reduced albedo, calculated from the diffusion pattern with $K^+/\Sigma_a<2$ and $K^-/\Sigma_a>2$: isotropic scattering (+) and Rayleigh-Gans scattering for $x=1(\Delta)$, 2(○), 5(+), 10(▲), and 20(●).

are given in Fig. 4, where K^+/Σ_a and K^-/Σ_a are presented as a function of c'. The results clearly show the difference with diffusion theory, which assumes $K^+/\Sigma_a=K^-/\Sigma_a=2$. It is remarkable that deviation with diffusion theory is even present for values of c' close to 1.

The results for values of $x>5$, where $g>0.9$, also coincide for K^+ and K^-. When assuming $S^+/K^+\approx S^-/K^-$, as suggested in Eq. (18), results for S^+ and S^- would also coincide for the phase functions with $g>0.9$.

3.5 *Internal Reflection at Boundaries*

Reflection occurs at boundaries when the refractive index of a scattering medium differs from that of the surrounding medium. The reflected fraction for a given angle of incidence with a smooth interface can be calculated with the Fresnel equations:

$$2R=\left[\frac{\sin(i-r)}{\sin(i+r)}\right]^2+\left[\frac{\tan(i-r)}{\tan(i+r)}\right]^2 , \tag{20}$$

with $\sin(i)/\sin(r)=n_r/n_i$, where i and r are the angles with the normal of the incident and refracted rays and n_i and n_r

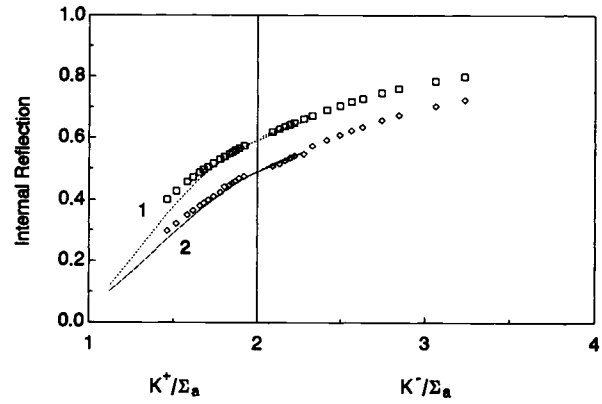

Fig. 5 Diffuse reflection at an interface with air as a function of K^+/Σ_a or K^-/Σ_a: 1—$n=1.5$ to $n=1.0$, 2—$n=1.33$ to $n=1.5$ to $n=1.0$. Lines: isotropic scattering, and symbols: Rayleigh-Gans scattering for $x=5$ and $x=20$.

are the refractive indices of both media. Internal reflection at an interface is much larger than specular reflection for normal incidence, and can be as large as 60% between a medium with a refractive index of 1.50 and air. The internal reflection at a given interface is therefore not only determined by the refractive indices at both sides of the interface but also by the angular diffusion pattern of the light approaching the interface.

The internal reflection at a smooth interface was calculated for the different diffusion patterns in the positive and negative direction in isotropic and anisotropic scattering. The results are given in Fig. 5 as a function of K^+/Σ_a or K^-/Σ_a. The first example describes internal reflection at an interface with air for a medium with $n_i=1.5$. The second example is given for reflection at a liquid-glass-air interface ($n=1.33$, 1.52, and 1.0, respectively), as occurs in a cuvette containing whole blood. It appears that the results for $g>0.9$ can be described with the equation

$$R^{(+/-)}=R_{\text{diff}}+0.65\ \ln[K^{(+/-)}/(2\Sigma_a)] , \tag{21}$$

excepted for values of K^+/Σ_a below 1.5. The internal reflection coefficient for the spherical diffusion pattern, R_{diff}, can be calculated without knowledge of the actual diffusion pattern. Application of Eq. (21) for smooth interfaces is allowed only if the angular intensity distribution at the interface is comparable with the diffusion pattern. Whether or not this can be assumed, might be concluded from the Monte Carlo simulations given in Sec. 4.

4 Monte Carlo Simulations

Some Monte Carlo simulations on slabs were performed for Rayleigh-Gans scattering and isotropic scattering. The results can be used to observe variations in K^+ and K^- at different positions within the slab to investigate the influence of boundaries; to verify the existence of similarity for $g>0.9$; and to determine the accuracy of the obtained results for K, S, K^+, and K^-. For these purposes, an option was implemented into a Monte Carlo program that we initially developed for simulating laser Doppler measurements of tissue perfusion.[1]

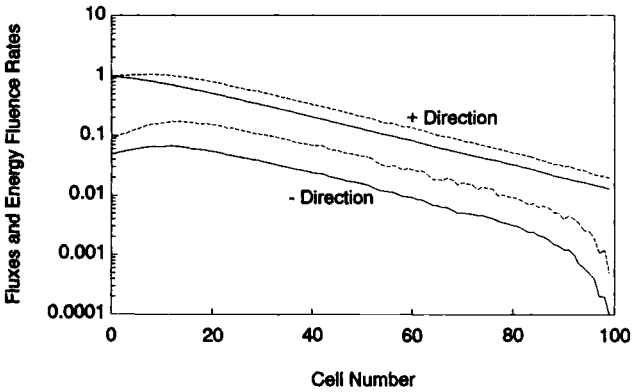

Fig. 6 Energy fluence rates (– – – –) and photon fluxes (——) in the positive and negative directions, both as a function of the position. Monte Carlo simulation for a slab. Rayleigh-Gans scattering, $c = 0.99$ and $x = 20$.

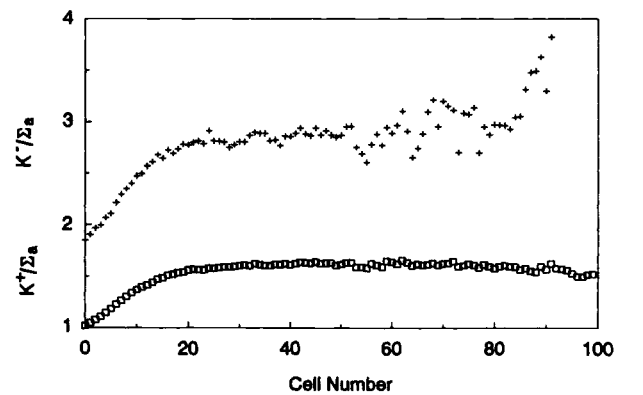

Fig. 7 Values for K^+/Σ_a (□) and K^-/Σ_a (+) as a function of the position in the slab. Monte Carlo simulation for a slab. Rayleigh-Gans scattering, $c = 0.99$ and $x = 20$.

For this study, a slab with a thickness of 5 mm was simulated with the modified program. Simulations were performed with incident radiation parallel to the z axis and with diffuse incident radiation. The slab was subdivided into 100 cells. For every cell, the contribution of the photon path length and its contribution in the z direction were added for photons traveling in the positive and negative directions separately. These sums were subsequently divided by the cell length and number of photons. In this way, energy fluence rates and photon fluxes I and J were determined. The ratio between the energy fluence rate and flux, both in the positive direction, equals K^+/Σ_a; the ratio in the negative direction equals K^-/Σ_a.

4.1 K^+ and K^- Near Boundaries

Monte Carlo simulations were performed with Rayleigh-Gans scatterers for which $c = 0.99$ and $x = 20$, with $\Sigma_a = 0.423\ \text{mm}^{-1}$, $\Sigma_s = 41.91\ \text{mm}^{-1}$, and $g = 0.9913$. The results for the fluxes and energy fluence rates for the case of a collimated input beam along the z axis are shown in Fig. 6. These results confirm an exponential behavior in a similar way as found in the unbounded medium, except in the vicinity of the boundaries.

Figure 7 shows the values for K^+/Σ_a and K^-/Σ_a that were obtained from Fig. 6 by calculating the ratio of the energy fluence rate and the flux in each cell for both directions. The value $K^+/\Sigma_a = 1$ in the first cell is caused by the normal incidence of the photons in the medium at $z = 0$. Note that K^+ increases until it practically remains constant for all further cells. The value of K^-, however, is high for the highest cell numbers, because the contribution of flux in the negative direction near the boundary is mainly caused by photons from the photon flux in the positive direction, initially having larger angles with the z axis.

The decrease of K^- in the vicinity of $z = 0$ is remarkable. We did not expect this decrease. The differences can be explained from the extremely forward scattering phase function for which the simulation has been performed: the contribution of backscattering from flux I to flux J for cell numbers below 20 can be neglected for the case of extremely forward scattering. Therefore, the emerging flux J at $z = 0$ mainly consists of photons from cell numbers above 20. Because the chance for absorption is large for the simulated case, this implies that photons propagating with a small angle with the z axis have a larger chance to reach $z = 0$ than the other photons, because their light paths are smaller.

4.2 Similarity and Accuracy

Monte Carlo simulations with the same values for Σ_a and Σ_s' and the same configuration were also performed for isotropic scattering and for Rayleigh-Gans scattering with $x = 5$ and thus $g = 0.9084$. Corresponding values for the scattering coefficient are $\Sigma_s = 0.365\ \text{mm}^{-1}$ and $\Sigma_s = 3.980\ \text{mm}^{-1}$, respectively.

Average values for α, K/Σ_a, K^+/Σ_a, and K^-/Σ_a between 2 and 3.5 mm for all simulations were derived from the Monte Carlo results as well as from the solution of the Boltzmann equation for the unbounded medium. Reflection and transmission, R and T, respectively, were also determined from the Monte Carlo simulations, as shown in Table 1.

Table 1 shows that the results from the solution of the Boltzmann equation are in better agreement with the Monte Carlo results than the predictions with the diffusion approximation. This is not surprising because the absorption coefficient is even larger than the reduced scattering coefficient for the given cases.

Table 1 also shows that all Monte Carlo simulation results for $x = 5$ and $x = 20$, including reflection and transmission, are similar. The Monte Carlo results for isotropic scattering differ from these values. This confirms the validity of similarity between results with high values of g.

The changes in K^-/Σ_a for small cell numbers that are shown in Fig. 7 for Rayleigh-Gans scattering with $x = 20$ were also observed for $x = 5$, but not for isotropic scattering. This also explains the increased reflection for isotropic scattering compared to Rayleigh-Gans scattering with $x = 5$ and $x = 20$.

It is remarkable that $\alpha_{\text{diff}}/\alpha$, as found from the ratio of Monte Carlo light fluxes at $x = 2$ mm and $x = 3.5$ mm, is smaller than expected from the solution of the Boltzmann equation for all simulations with a collimated input beam. This difference is much smaller when diffuse incident radiation is applied, as shown in Table 1. Therefore, we expect that a remaining fraction of collimated light in the positive direction might be responsible for this difference,

Table 1 Results for Monte Carlo simulations of light propagation in a 5-mm slab for Rayleigh-Gans scatterers (RG), with $x=5$ ($g=0.9913$) and $x=20$ ($g=0.9084$), and for isotropically (is) scattering ($g=0$): $\Sigma_a=0.4233\ \text{mm}^{-1}$ and $\Sigma_s(1-g)=0.365\ \text{mm}^{-1}$. The slab is surrounded by a medium with the same refractive index. Tabulated values for α_{diff}/α, K/Σ_a, K^+/Σ_a, and K^-/Σ_a are average values between 2.0 and 3.5 mm. R = total reflection, T = total transmission, and N = number of simulated photons.

	α_{diff}/α	K/Σ_a	K^+/Σ_a	K^-/Σ_a	R	T	N
Monte Carlo Simulations with illumination parallel to z-axis:							
Rayleigh-Gans,x=20	1.08	1.75	1.62	2.90	0.047	0.013	30000
Rayleigh-Gans,x=5	1.16	1.70	1.59	2.83	0.052	0.016	30000
Isotropic	1.42	1.33	1.23	2.17	0.104	0.031	30000
Monte Carlo Simulations with diffuse illumination:							
Rayleigh-Gans,x=20	1.04	1.75	1.63	2.80	0.103	0.009	30000
Rayleigh-Gans,x=5	1.14	1.70	1.60	2.70	0.097	0.011	30000
Isotropic	1.27	1.46	1.36	2.30	0.118	0.018	30000
Boltzmann equation, unbounded medium:							
Rayleigh-Gans,x=20	1.12	1.72	1.61	2.92	-	-	-
Rayleigh-Gans,x=5	1.13	1.70	1.59	2.83	-	-	-
Isotropic	1.31	1.43	1.34	2.25	-	-	-
Diffusion approximation:							
Isotropic	1.00	2.00	2.00	2.00	-	-	-

especially for the case of isotropic scattering. In that case, the attenuation of the collimated beam, $\Sigma_a+\Sigma_s=0.79\ \text{mm}^{-1}$, is close to $\alpha=0.76\ \text{mm}^{-1}$.

The reliability of the numerical procedure for α for anisotropic scattering was verified by solving the Boltzmann equation for Henyey-Greenstein scattering. No differences between data for α from Table 23 of Van de Hulst[11] have been observed.

The remaining differences between Monte Carlo simulations and the solution of the Boltzmann equation can therefore probably be attributed to inaccuracy in the Monte Carlo results caused by interpolation procedures in the tabulated phase function. The results with $x=20$ are most sensitive to this source of inaccuracy, because the intensity decreases very rapidly for increasing small scattering angles.

5 Discussion and Conclusions

It has been shown that the solution of the Boltzmann equation obtained in our study gives improved results compared with the diffusion approximation. The absorption and backscattering coefficients K and S can be calculated from a numerical solution of the Boltzmann equation, as shown for Rayleigh-Gans scattering, when assuming $K=K^+=K^-$ and $S=S^+=S^-$. However, the results for K and S are different for the positive and negative directions, even for values of c' close to 1.0.

Our numerical procedures for solving the Boltzmann equation were verified by comparison with published data. Results for α and K, using isotropic scattering, are in agreement with the data of α and K, as given by Klier,[20] as shown earlier.[14] Agreement was also shown for anisotropic scattering by comparison with results for Henyey-Greenstein scattering of Van de Hulst.[11]

The major conclusion of this study is that similarity between the results for Rayleigh-Gans scatterers with $g>0.9$ exists for α_{diff}/α, K/Σ_a, $S/[\Sigma_s(1-g)]$, K^+/Σ_a, and K^-/Σ_a in the unbounded medium, independent of c'. This implies that separate knowledge of Σ_s and g is less important in that range when Σ_s' is known. This principle of similarity for Rayleigh-Gans scatterers can be applied for all values of the reduced albedo only as long as both values of g are above 0.9. For smaller values of g, similarity becomes less, especially for lower values of c'. Similarity between forward scattering Rayleigh-Gans phase functions and isotropic scattering is even restricted to $c'\approx 1$.

Similarity also holds for the internal diffuse reflection, because it can be described as a function of the diffuse reflection and K^+/Σ_a or K^-/Σ_a. The internal diffuse reflection in the positive direction can be calculated from the diffusion pattern with Eq. (21), because K^+/Σ_a does not change much near the boundary, as can be concluded from the behavior of K^+/Σ_a in Fig. 7.

The internal reflection for light propagating in the negative direction cannot be calculated from the diffusion pattern. For the case of Fig. 7, it will be less, because the flux at $z=0$ is directed more parallel with the z axis than it is farther from the boundary. However, similarity for $g>0.9$ has also been observed for K^-/Σ_a near the boundary, whereas results for isotropic scattering are different. Therefore, it can be concluded that similarity can be extended to situations where boundary conditions are important.

Earlier we suggested that results obtained with the solution of the Boltzmann equation might be used to improve existing models, such as two- and four-flux models and diffusion theory.[14] However, it might not be easy to implement the behavior, as observed in Fig. 7, into such simple analytical models. Many-flux models[19] and adding-doubling methods,[12] therefore, probably remain superior for the analytical approach of slabs, and Monte Carlo simulations for configurations where no accurate analytical solution is available.

The similarity principle also has important advantages in Monte Carlo studies. It can reduce the number of Monte Carlo simulations needed to characterize light propagation in turbid media where $g>0.9$. Moreover, similarity can be used to decrease the amount of calculation time needed for a Monte Carlo simulation on highly forward scattering media such as biological tissues: the mean free path can be increased considerably by choosing a value of g as low as possible. Calculation of a photon path can be performed much faster in that way.

This study was performed for Rayleigh-Gans scattering and isotropic scattering only. The validity of similarity for other scatterers with high values of g can also be found in results of Van de Hulst[11] and in Monte Carlo simulations of Star et al.,[13] both for Henyey-Greenstein scattering.

Note, however, that extension of our conclusions concerning similarity to other phase functions with high values for g should be performed only with care. A phase function with $g>0.9$ can also be derived by the addition of forward peaked scattering to isotropic scattering. However, there is no difference between forward scattering and no scattering, and thus this type of anisotropic scattering can be reduced

to isotropic scattering with the same value of c'. Consequently, similarity for $c' \ll 1.0$ does not hold, because isotropic scattering does not behave similarly to Rayleigh-Gans scattering with $g > 0.9$, as shown.

Similarity probably requires that f_1 and higher terms f_i, of Eq. (8), should have values that do not deviate too much between both phase functions, especially when $c' \ll 1$. When $g > 0.9$, the Henyey-Greenstein and Rayleigh-Gans phase functions have relatively high values for f_i, as shown in Sec. 2.2 and in Fig. 6 of Ref. 14. For isotropic scattering, however, $f_i = 0$ for $i > 0$.

Many biomedical applications involve uncertainty concerning the phase function. Tissues and blood are both extremely forward scattering media. Values for g between 0.98 and 0.995 for blood have been reported.[7] Reported values for tissues are in the range[21] 0.7 to 0.9 or higher.[22] Therefore, it is to be expected that similarity can be applied to biological tissues. However, some uncertainty still remains in this case, because the phase functions of these scatterers might differ from Rayleigh-Gans and Henyey-Greenstein phase functions. A worst case estimate of the uncertainty in the prediction of light propagation in the medium with respect to the phase function might, therefore, be obtained by comparing the results for Rayleigh-Gans scattering and isotropic scattering with the same value of c'.

In summary, when comparing highly forward scattering to Monte Carlo simulations for isotropic scattering, or by using diffusion theory, it is not possible to use similarity far from $c' \approx 1$. However, for spherical Rayleigh-Gans scattering with $g > 0.9$ similarity with validity for all values of the reduced albedo has been discovered. This implies that the number of variables that describe light propagation can be reduced for all values of Σ_a. When used in Monte Carlo simulations, similarity has the advantage that simulations for other values of g in that range can be omitted, also when $c' \ll 1$.

References

1. H. W. Jentink, F. F. M. de Mul, R. G. A. M. Hermsen, R. Graaff, and J. Greve, "Monte Carlo simulations of laser Doppler blood flow measurements in tissue," *Appl. Opt.* **29,** 2371–2381 (1988).
2. M. Cope and D. T. Delphy, "System for long-term measurement of blood and tissue oxygenation on newborn infants by near infra-red transillumination," *Med. Biol. Eng. Comp.* **26,** 289–294 (1988).
3. Y. Shimada, I. Yoshiya, and N. Oka, "Effects of multiple scattering and peripheral circulation on arterial oxygen saturation measured with a pulse-type oximeter," *Med. Biol. Eng. Comput.* **22,** 475–478 (1984).
4. Y. Mendelson and B. D. Ochs, "Noninvasive pulse oximetry utilizing skin reflectance photoplethysmography," *IEEE Trans. Biomed. Eng.* **35,** 798–805 (1988).
5. A. C. M. Dassel, R. Graaff, J. G. Aarnoudse, J. M. Elstrodt, P. Heida, M. H. Koelink, F. F. M. de Mul, and J. Greve, "Reflectance pulse oximetry in fetal lambs," *Pediatr. Res.* **31,** 266–269 (1992).
6. R. P. Hemenger, "Optical properties of turbid media with specularly reflecting boundaries: applications to biological problems," *Appl. Opt.* **16,** 2007–2012 (1977).
7. L. Reynolds, C. Johnson, and A. Ishimaru, "Diffuse reflectance from a finite blood medium: applications to the modeling of fiber optic catheters," *Appl. Opt.* **15,** 2059–2067 (1976).
8. R. A. J. Groenhuis, H. A. Ferwerda, and J. J. Ten Bosch, "Scattering and absorption of turbid materials determined from reflection measurements. 1: Theory," *Appl. Opt.* **22,** 2456–2462 (1983).
9. J. M. Steinke and A. P. Shepherd, "Diffusion model of the optical absorbance of whole blood," *J. Opt. Soc. Am. A* **5**(6), 813–822 (1988).
10. S. T. Flock, B. C. Wilson, and M. S. Patterson, "Hybrid Monte Carlo—diffusion theory modelling of light distributions in tissue," in *Laser Interaction with Tissue, Proc. SPIE* **908,** 20–28 (1988).
11. H. C. Van de Hulst, *Multiple Light Scattering, Tables, Formulas and Applications,* Vols. 1 and 2, Academic Press, New York (1980).
12. S. A. Prahl, "Calculation of light distributions and optical properties in tissue," PhD Dissertation, Dept. of Biomed. Eng., Univ. of Texas, Austin (1989).
13. W. M. Star, J. P. A. Marijnissen, and M. J. C. van Gemert, "Light dosimetry in optical phantoms and in tissues: I. Multiple flux and transport theory," *Phys. Med. Biol.* **33**(4), 437–454 (1988).
14. R. Graaff, J. G. Aarnoudse, F. F. M. de Mul, and H. W. Jentink, "Light propagation parameters for anisotropically scattering media, based on a rigorous solution of the transport equation," *Appl. Opt.* **28,** 2273–2279 (1989).
15. J. R. Mika, "Neutron transport with anisotropic scattering," *Nucl. Sci. Eng.* **11,** 415–427 (1961).
16. K. M. Case and P. F. Zweifel, *Linear Transport Theory,* Addison-Wesley, Reading, Mass. (1968).
17. M. Abramowitz and I. A. Stegun, *Handbook of Mathematical Functions,* Dover, New York (1965).
18. V. I. Haltrin, "Exact solution of the characteristic equation for transfer in the anisotropically scattering and absorbing medium," *Appl. Opt.* **27**(3), 599–602 (1988).
19. P. S. Mudgett and L. W. Richards, "Multiple scattering functions for technology II," *J. Colloid Interface Sci.* **39,** 551–567 (1972).
20. K. Klier, "Absorption and scattering in plane parallel turbid media," *J. Opt. Soc. Am.* **62,** 882–885 (1972).
21. M. J. C. van Gemert, S. L. Jacques, H. J. C. M. Sterenborg, and W. M. Star, "Skin optics," *IEEE Trans. Biomed. Eng.* **36,** 1146–1154 (1989).
22. S. T. Flock, "Total attenuation coefficients and scattering phase functions of tissues and phantom materials at 633 nm," *Med. Phys.* **14**(5), 835–841 (1987).

Reindert Graaff received his MS in technical physics at the Technical University of Delft in 1979 and joined the Research Laboratory of Nederlandse Gasunie where he worked on modeling two-phase flow behavior in gas-condensate pipelines. In 1986, he joined the University of Groningen, Faculty of Medicine, for the development of reflection pulse oximetry. He is interested in the application of tissue optics in noninvasive measuring methods in medicine.

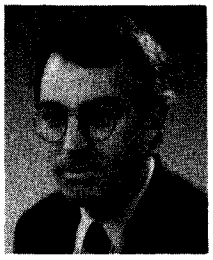

Jan G. Aarnoudse received his MD at the University of Groningen in 1969. He started his training in obstetrics and gynecology at the University Hospital in Groningen in 1971, and finished it in Curaçao, Dutch Antilles, in 1976. He returned to Groningen, where he received his PhD in 1980 on an experimental and clinical study of the measurement of subcutaneous oxygen tensions in the fetus with a needle electrode. From 1980 to 1981 he joined Prof. Frank Hytten at the Clinical Research Centre in London, where he studied placental perfusion. In 1981 he returned to the Department of Obstetrics and Gynecology of the University of Groningen as an associate professor and became professor in obstetrics and perinatal medicine in 1988. His current interests are fetal Doppler ultrasound and noninvasive optical monitoring.

Frits F. M. de Mul obtained his MS and PhD at the Technical University of Delft, Department of Applied Physics, in 1966 and 1973, respectively, on the subject of neutron physics. After a short period of teaching in a secondary school, he joined the University of Twente, Department of Applied Physics, primarily for teaching, but since 1981 has also been a senior scientist in the Technical Optics/Biophysical Technology group, where he is involved in instrumentation, light scattering, and biomedical optics.

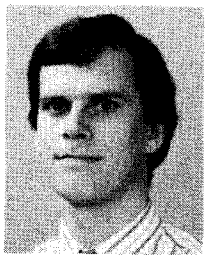

Henk W. Jentink received his MS in experimental physics at the University of Leiden, The Netherlands, in 1984. He joined the Netherlands Technology Foundation studying laser Doppler anemometry using diode lasers. He focused on the biomedical applications of the technique. In 1989 he received his PhD for this work at the University of Twente. Currently he is developing instrumentation for flight-test purposes at the National Aerospace Laboratory in The Netherlands. His current interests include optical measuring techniques and optical sensors.